Macromolecular Research

Article

DOI 10.1007/s13233-020-8169-y

www.springer.com/13233 pISSN 1598-5032 eISSN 2092-7673

Waste Sawdust-Derived Nanoporous Carbon as a Positive Electrode for Lithium-Ion Storage

Jin Hwan Kwak[†,1]
Jong Chan Hyun[†,2]
Seong Bak Moon[3]
Hyoung-Joon Jin[3]
Hee-Dae Lim[1,4]
Young Soo Yun[*,2]

[1] Center for Energy Storage Research, Korea Institute of Science and Technology (KIST), Hwarangro 14-gil 5, Seoungbuk-gu, Seoul 02792, Korea
[2] KU-KIST Graduate School of Converging Science and Technology, Korea University, 145 Anam-ro, Seongbuk-gu, Seoul 02841, Korea
[3] Department of Polymer Science and Engineering, Inha University, Incheon 22212, Korea
[4] Division of Energy & Environment Technology, KIST School, Korea University of Science and Technology, Seoul 02792, Korea

Received June 22, 2020 / Revised October 25, 2020 / Accepted October 26, 2020

Abstract: Sustainable resources, particularly those induced from bio-derived waste materials, can be transformed into useful nanocarbon materials with high functionality. In this study, nanoporous carbon materials (N-CMs) were fabricated from waste sawdust using a simple heating process and a carefully controlled activation process. The waste-induced N-CMs had a high specific surface area of ~3044.6 $m^2 g^{-1}$, a nanoporous structure, and > 6 at.% heteroatoms. These properties led to high electrochemical performance with a specific capacity of ~298 mAh g^{-1} and excellent cycling stability over 2,000 cycles as a cathode in lithium-ion storage. Moreover, when the N-CMs were assembled with a nanostructured carbon-based anode, all full carbon-based cells could deliver high specific energy and specific power of ~377 Wh kg^{-1} and ~20,247 W kg^{-1}, respectively, with a long-term cycle life of more than 1,000 cycles.

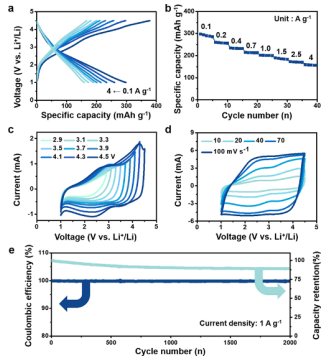

Keywords: nanoporous carbon, pseudocapacitance, cathode, waste biomass, Li-ion, upcycling.

1. Introduction

With the rapid advances in modern society, the demands for cutting-edge technologies, such as portable electronic devices and electric vehicles, have been increasing. Accordingly, studies to develop high-performance energy storage devices (ESDs) are being carried out.[1,2] Several types of rechargeable batteries, including well-known lithium-ion batteries (LIBs), have been reported. Multivalent ion batteries, metal-air/sulfur/carbon dioxide batteries, and alkali metal batteries have also attracted considerable attention as a high energy density ESD.[3-8] On the other hand, the new types of ESDs have many obstacles to overcome, such as low round-trip energy efficiencies, poor cycling stabilities, and safety issues.[9,10] In addition, an increase in the lithium supply and the development of infra technology in the LIB system have led to the sustainable expansion of LIB markets, requiring more advanced LIBs with higher energy and power densities as well as longer-term cycling performance.

The electrochemical performance of LIBs is strongly dependent on the properties of active electrode materials (AEMs) because they play a key role as a charge storage host. Conventional cathode materials, such as lithium cobalt oxide and lithium manganese oxide, are based mainly on an intercalation reaction, in which a lithium-ion is inserted in a designated site within the crystal lattice (host structures).[11] Transition metal oxide (TMO)-based cathode materials can deliver a specific capacity of approximately 150~200 mA h g^{-1} in a high redox potential of approximately 3.5~4.0 V *vs.* Li^+/Li with stable cycling behavior, while they suffer from significantly low kinetic performance and inadequate cycling behaviors.[12] In addition, TMOs, including high oxygen contents, are flammable and relatively expensive, requiring an alternative AEM with high-performance, superb safety, and mass-scalability.[13] On the other hand, nanoporous carbon-based materials (N-CMs) are promising AEMs owing to their high specific active surface area, good electrical conductivity, and chemical stability.[14,15] In the nanoporous structure, a large amount of charges can be accumulated by forming electrochemical double layers.[16,17] In addition, defective structures on N-CMs can be a redox host for pseudocapacitive charge storage.[18] These charge storage behaviors show significantly stable cycle lives because they mainly happen on the surface and/or near surface of N-CMs with no volume change. Moreover, the very easy and inexpensive fabrication process based on bio-abundant polymer precursors and simple heating methods make N-CMs more attractive as AEMs for LIBs.[19] Furthermore, the material properties of N-CMs can be tuned simply by controlling the pyrolysis conditions and precursor

Acknowledgment: This research was conducted with fundings of the National Research Foundation of Korea (NRF) (Nos. 2019R1A2C1084836 and 2018R1A4A1025169).

***Corresponding Author:** Young Soo Yun (c-ysyun@korea.ac.kr)
[†]The authors served equally to this study.

materials.[20,21] Therefore, several types of bio-induced polymer materials, such as ginkgo leaf, coconut oil, fungus, and sweet potato, have been used as a precursor for N-CMs. They have been applied actively as an anode for LIBs, but there are few reports of their use as a cathode.[22-26]

In this study, high-performance N-CMs as a positive electrode for Li ion storage were developed from bio-waste by simple fabrication method. Lignocellulosic biomass-derived waste, waste sawdust, was used as a precursor to fabricate the N-CM because cellulose-based natural resources can be pyrolyzed into carbonaceous materials with a balance of sp^3 carbon defects and oxygen functional groups. N-CM-6s have a high specific surface area of 3044.6 m^2 g^{-1} and a large number of nanopores with oxygen functional groups, showing outstanding electrochemical performance in a cathodic voltage region of 1.0~4.5 V *vs.* Li^+/Li. In addition, they delivered 298 mAh g^{-1} at a current density of 0.1 A g^{-1} that was maintained for more than 2,000 cycles at a current density of 1 A g^{-1} with capacity retention of 89%. Moreover, the N-CM-based full cells demonstrated feasible electrochemical performance with a specific energy density of ~377 Wh kg^{-1}.

2. Experimental

2.1. Preparation of N-CMs

Waste-sawdust was obtained from a furniture factory around Korea University. The sawdust was ground to a fine dust before the two-step heat-treatment process. The resulting sawdust was heated to 600 °C at a heating rate of 10.0 °C min^{-1} for 2 h under a N_2 atmosphere in a tubular furnace to obtain the lignocellulose-derived carbonaceous materials.[27] After the first heating process, the carbonaceous sawdust was heated with potassium hydroxide (KOH) in a tubular furnace to 800 °C at a heating rate of 10.0 °C min^{-1} under a N_2 atmosphere. The amount of KOH to the carbonaceous sawdust was 400, 600, and 800%. The products were purified thoroughly with distilled water and ethanol and stored in a vacuum oven at 80 °C. The products, N-CMs, are called N-CM-4, N-CM-6 (WSD-N-CMs), and N-CM-8 according to the weight ratio of KOH.

As an anode material for the full cell test, bacterial cellulose (BC) hydrogels were synthesized using *Acetobacter xylinum* BRC 5 in Hestrin and Schramm medium according to a previously reported process.[28] Before the freeze-drying process, the BC hydrogels were immersed in tert-butanol to exchange the solvents. The BCs were freeze-dried at -45 °C and 4.5 Pa for 3 days, resulting in a white color cryogel. The BC cryogel was pyrolyzed to 800 °C for 2 h at a heating rate of 2 °C min^{-1} under an inert gas (nitrogen) flow rate of 3 mL s^{-1}. The resulting sample was stocked in a vacuum oven at 30 °C.

2.2. Characterization

Materials properties of N-CM samples and their electrochemical analysis methods were described in Supporting Information.

3. Results and discussion

The morphologies of N-CM-6s were examined by field-emission scanning electron microscopy (FE-SEM) and field-emission transmission electron microscopy (FE-TEM). FE-SEM revealed an interconnected macroporous structure (Figure 1(a)), and TEM indicated that N-CM-6s have a fully amorphous carbon-ring structure with poor graphitic ordering (Figure 1(b) and Figure S1). The microstructural features are also supported by the X-ray

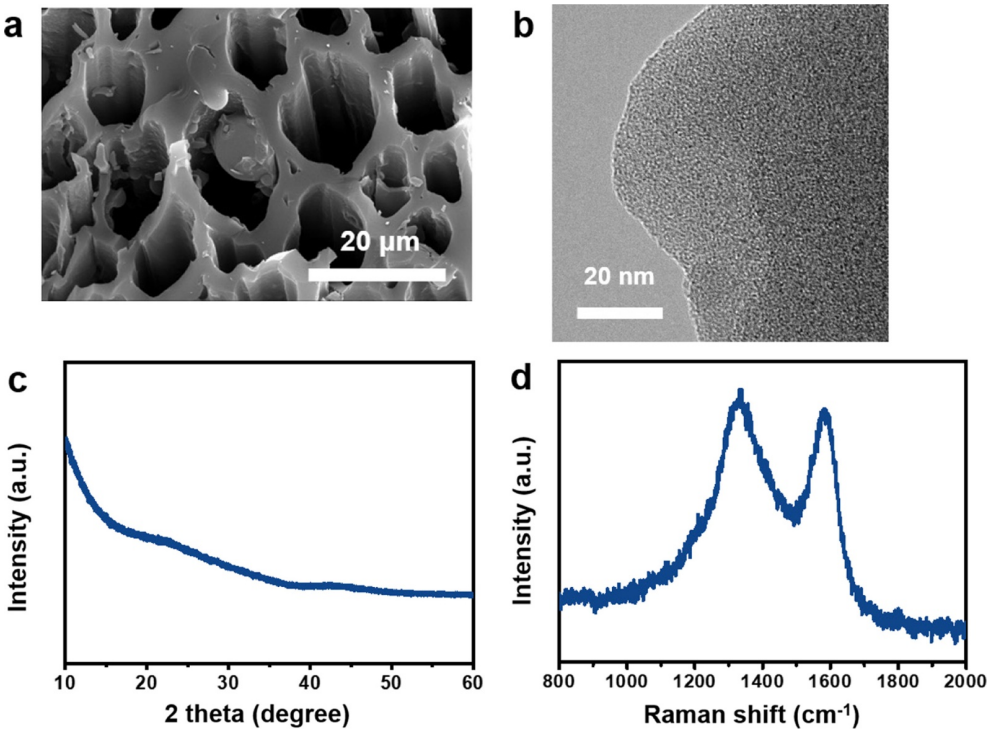

Figure 1. Morphology and microstructure of N-CM-6: (a) FE-SEM image; (b) FE-TEM image; (c) XRD pattern, and (d) Raman spectrum.

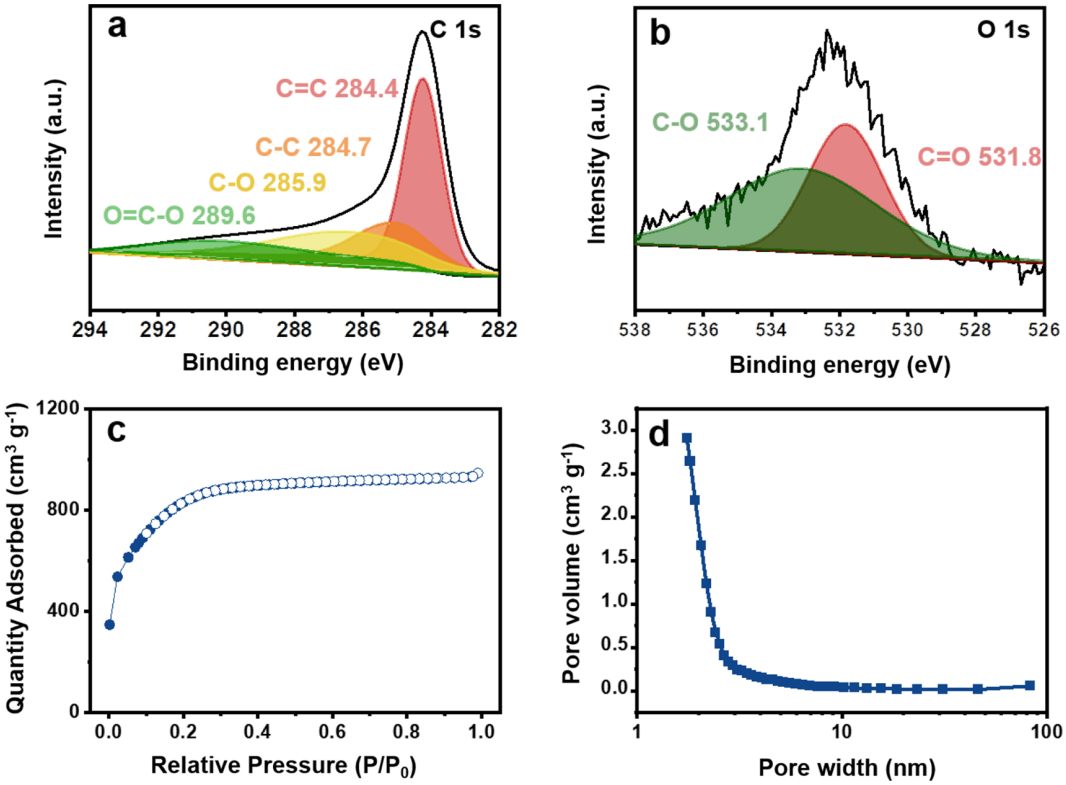

Figure 2. Materials properties of N-CM-6s: (a) XPS C 1s spectra; (b) XPS O 1s spectra; (c) Nitrogen-adsorption and desorption isotherm curves; (d) pore size distribution data.

diffraction (XRD) data, which revealed a broad (002) graphite peak, meaning that N-CM-6s is composed of a basic structural unit with short-range ordering (Figure 1(c)). In addition, as shown in Figure 1(d), the Raman spectra exhibited distinct *D* and *G* bands at ~1,348 and ~1,580 cm^{-1}, respectively. The *D* band corresponds to the asymmetric A_{1g} breathing mode of the poly-hexagonal ring structure, and the *G* band originates from the E_{2g} vibration mode of the crystals related to conjugated carbon atoms. Therefore, the similar intensity ratio of the *D* to *G* band shows that N-CM-6s are composed of a few nanometer-sized symmetric hexagonal carbon-ring structures with a number of defect sites.

The surface chemical properties were also characterized by X-ray photoelectron spectroscopy (XPS), as shown in Figure 2(a) and 2(b). In the C 1s spectra, C=C bonding centered at 284.4 eV was observed. Minor C-C bonding (285.1 eV), C-O bonding (286.4 eV), and O=C-O (288.4 eV) were also noted (Figure 2(a)). In the O 1s spectra, distinct C=O bonding and C-O bonding were found at 531.5 and 533.0 eV, respectively. Table 1 lists the atomic ratio of C, N, and O. The large number of heteroatoms of N-CM-6s can act as pseudocapacitive charge storage hosts that can sharply increase their specific capacities. The nitrogen-based isothermal test results of the N-CM-6s revealed a high specific surface area of 3044.2 $m^2 g^{-1}$ (Figure 2(c)). The shape of BET data was similar to IUPAC type-I, meaning that N-CM-6s consists mainly of micropores. The pore size distributions (PSDs) also indicate that N-CM-6s have numerous nanopores (< 2 nm) (Figure 2(d)). Table 1 lists the textural properties of all samples fabricated with 400 and 800% weight ratio of KOH to the precursor sample.

Electrochemical tests were performed to characterize the properties of N-CM-6s in a lithium-based electrolyte using an automatic battery cycler from Wonatech and a 2032-type coin cell. In the half-cell test, lithium metal foil was used as a counter and reference electrode. The mass loading of N-CMs was ~0.6 mg cm^{-2}. The galvanostatic charge/discharge curves showed that N-CM-6s could deliver a discharge capacity of 298 mA h g^{-1} and 159 mA h g^{-1} at a current density of 0.1 A g^{-1} and 4 A g^{-1}, respectively, under the voltage range from 1.0 to 4.5 V *vs.* Li^+/Li (Figure 3(a), (b)). From the linear profiles, the charge storage mechanism of N-CM-6s was considered to be surface-driven charge storage behavior, mainly a pseudocapacitive reaction that occurred at the edge

Table 1. Microstructure and chemical properties of N-CM-6s characterized by BET and XPS

Sample name	Specific surface area ($m^2 \cdot g^{-1}$)			Atomic ratio (%)		
	S_{BET}[a]	S_{Mic}[b]	S_{Ext}[c]	C	O	N
N-CM-4s	2776.5	2588.2	188.3	91.1	8.7	0.2
N-CM-6s	3044.6	2861.2	183.3	93.1	5.9	1.0
N-CM-8s	2312.8	2111.6	201.1	93.3	5.6	1.1

[a]BET surface area, [b]surface area of micropore and [c]surface area except micropore.

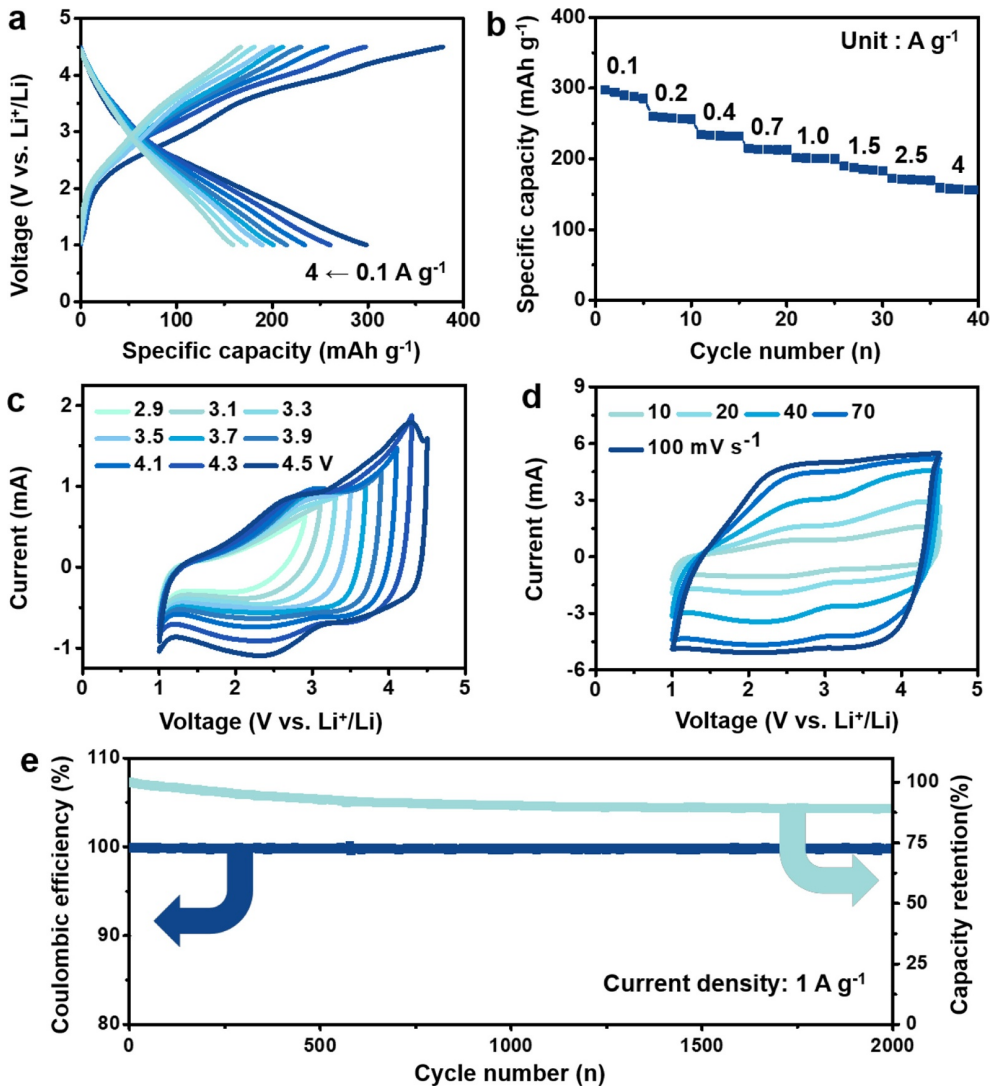

Figure 3. Electrochemical performance of N-CM-6s in a cathodic voltage region for lithium-ion storage: (a) Galvanostatic charge/discharge profiles; (b) rate capabilities at various current rates; (c) cyclic voltammograms at different voltage ranges from 2.9 to 4.5 V *vs.* Li^+/Li at a scan rate of 0.1 V s^{-1}; (d) CV curves of N-CM-6s at various scan rates; (e) cycling performances at a current density of 1 A g^{-1} over 2,000 cycles.

defects and the heteroatoms as a redox host. In addition, the rapid Li-ion transport induced from the surface-driven reaction results in good rate performance.[29] To characterize the surface-driven storage mechanism in more detail, cyclic voltammetry (CV) was conducted at voltages ranging from 2.9 to 4.5 V (Figure 3(c)). In the CV curves, no sharp peaks related to a redox reaction were noted, indicating that the charge storage behaviors progressed without the formation of any new phase as a one-phase reaction, which is dependent mainly on the chemical potential of lithiated active carbon materials. Moreover, large increases in pseudocapacitance were observed with increasing voltage range. Basically, the physical adsorption and desorption behaviors of charge carriers by electrochemical double layer formation showed constant current at the given scan rate, whereas the CV curves on N-CM-6s exhibited a continuous current, indicating the presence of additional charge storage behaviors. The additional charge storage behaviors can be interpreted as pseudocapacitance because the redox reaction on carbon-based materials have a large voltage hysteresis between the adsorption and desorption reaction. Therefore, with a larger operating voltage window, more pseudocapacitance values can be achieved, as shown in Figure 3(c). The CV profiles also provided key information that the pseudocapacitance has high rate capability (Figure 3(d)). The CV curves characterized at a range of scan rates from 0.01 to 0.1 V s^{-1} exhibited similar rectangular-like shapes, indicating great rate capabilities. In addition, in a cycling test at a current density of 1 A g^{-1}, a Coulombic efficiency of 99%, and capacity retention of 89% were maintained over 2,000 cycles (Figure 3(e)), indicating highly reversible surface-driven charge storage behavior. To further prove the cycling stability of N-CM-6s, additional comparative analysis was performed (Figure S1). After the repeated 2,000 cycles, a slight change of carbon structures was observed, and inactive byproducts were accumulated on the electrode surface (Figure S2a, S2b). Because of the presence of non-conducting products, a charge transport resistance (R_{ct}) of N-CM-6s was increased from ~15 to 50 Ω after the long-term cycling (Figure S2c). Nevertheless, the macroporous structure is well-maintained, and the equivalent series resistance of N-

Table 2. Electrochemical performances of previously reported carbon-based positive electrodes

Samples	Working voltage (V)	Specific capacity	Cycle life	Ref.
rGO-CNT	2.0-4.0	63 mAh g^{-1} (0.2 A g^{-1})	280 cycles (1 A g^{-1})	[30]
CPAC-5	2.0-4.5	135 mAh g^{-1} (0.5 A g^{-1})	2,000 cycles (1 A g^{-1})	[31]
YP	2.0-4.0	66 mAh g^{-1} (0.01 A g^{-1})	500 cycles (0.1 A g^{-1})	[32]
PG	2.0-4.5	69 mAh g^{-1} (0.1 A g^{-1})	3,000 cycles (1 A g^{-1})	[33]

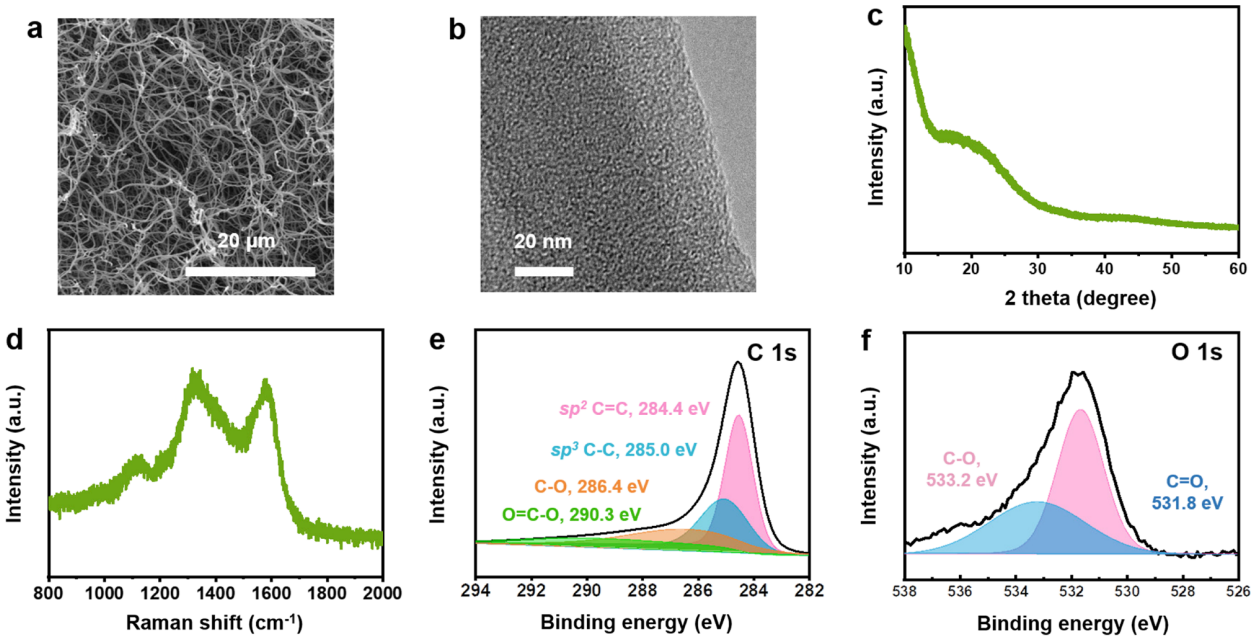

Figure 4. Material characterization of BNCs: (a) SEM image; (b) TEM image; (c) XRD data; (d) Raman spectra; (e) XPS C 1s spectra; (f) XPS O 1s spectra.

CM-6s is still below ~70 Ω after the cycling. Considering the significantly long cycling process, these morphological changes and piling up of small amount of byproducts seem to be an acceptable level. Therefore, the highly stable cycling behaviors can be achieved during the long-term cycling process. The superiority of N-CM-6s on electrochemical performances was also confirmed by comparing them with the previously reported results.[30-33]

Through full-cell tests, the feasibility of N-CM-6s as an active cathode material was investigated. BC-derived nanoweb-carbons (BNCs) were selected as the anode material because they have well-balanced energy and power performance. The materials properties of BNCs were characterized, as shown in Figure 4. FE-SEM showed that BNCs have a three-dimensional nanoweb structure, which is an advantageous structure to provide them with several charge diffusion channels (Figure 4(a)). In addition, FE-TEM, XRD, and Raman spectroscopy of the BNCs indicated they have a fully amorphous six-membered carbon structure without long-range graphitic ordering (Figures 4(b)-(d)). The chemical structure of BNCs supports the characterization results; the C 1s spectrum revealed mainly sp^2 C=C and sp^3 C-C bonding structures with a few oxygen heteroatoms that have C-O and/or C=O bonding (Figure 4(e), (f)). Hence, BNCs have an amorphous nanostructure and some hydrophilic functional groups that assist in wettability in the carbonate-based electrolyte.

Galvanostatic charge/discharge profiles of BNCs show that they can deliver a high specific capacity of 317 mAh g^{-1} at a current density of 0.1 A g^{-1} with high reversibility (Figure 5(a)). The galvanostatic charge/discharge profiles are linear shapes, indicating that the BNCs also store charge by a surface-driven mechanism. The specific capacities were maintained by ~110 mAh g^{-1}, even at an 80 times higher current density corresponding to 8 A g^{-1} (Figure 5(b)). In addition, the high Coulombic efficiency of 99% and capacity retention of 77% after 1,000 cycles at a current density of 1 A g^{-1} are noteworthy results (Figure 5(c)). The specific capacities and rate capabilities of BNCs are similar to those of N-CM-6s, suggesting that they can be an excellent electrode pair with well-balanced energy and power performance.

To assemble an optimized full cell, full-cell tests were performed after pre-cycling several cycles at a half-cell configuration with the same electrolyte system. In the pre-cycling process, the open-circuit voltage of the half-cell was fixed to 1.5 V *vs.* Li^+/Li. Figure 4(d) shows a schematic diagram of the respective galvanostatic charge/discharge profiles of the anode and cathode, which starts at 1.5 V *vs.* Li^+/Li as an onset voltage and operates in a voltage gap between 0.5 and 4.5 V. As shown in Figure 5(e), the full-cells can deliver a specific capacity of 211 and 149 mAh g^{-1} at a current density 0.2 and 8 A g^{-1} (even at a 40 times higher rate), respectively. The rapid charge/discharge behaviors suggest that they have a good balance in rate capabilities. As shown in the Ragone plot, the energy density and power density of the full-cell were higher than those of ESDs based on the carbon cathodes (Figure 5(f)).[34-36] The cycling performance of the full-cell was examined at a

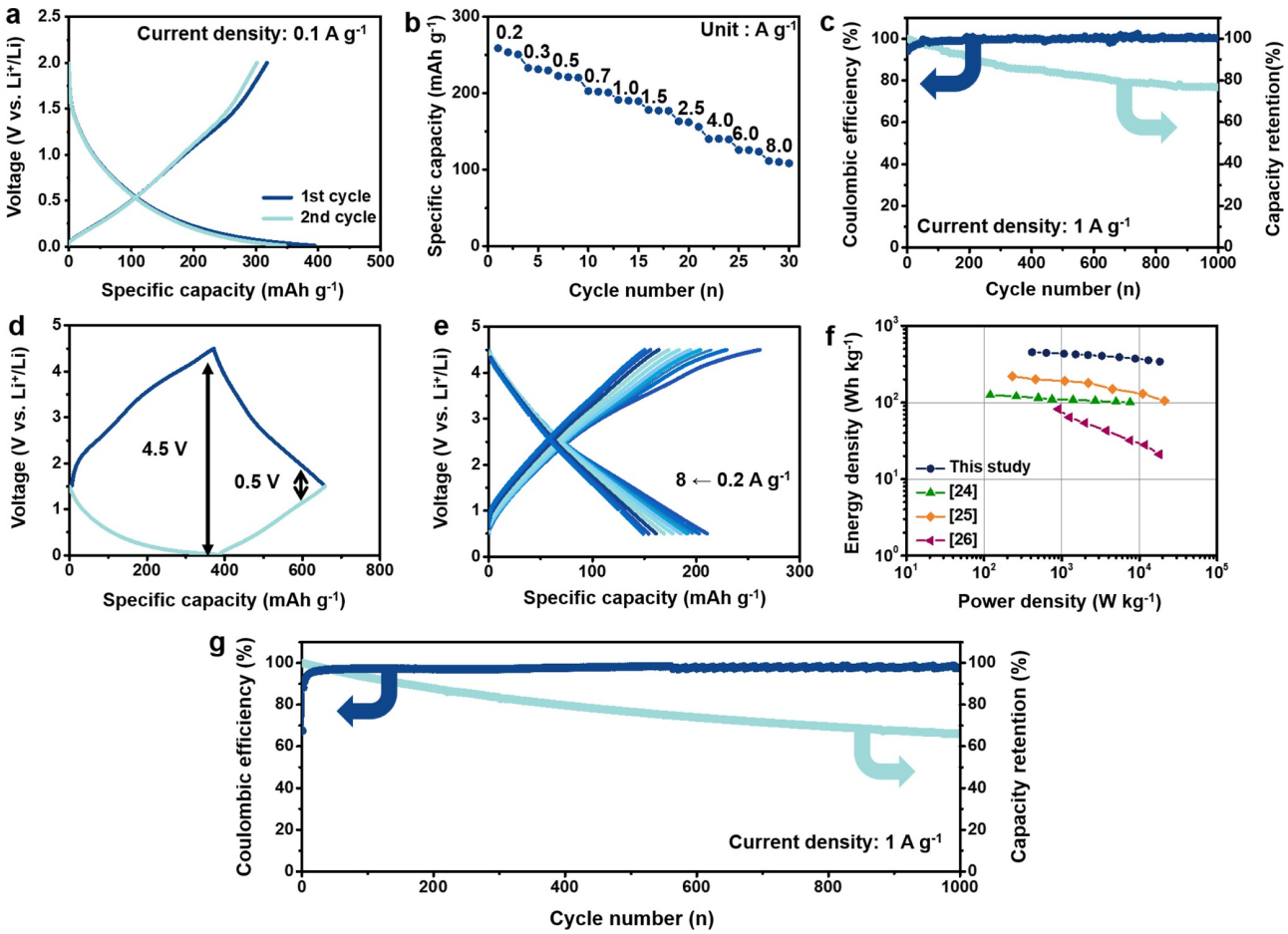

Figure 5. Electrochemical performances of BNC anode and BNC//N-CM-6s full cells: (a) Galvanostatic charge/discharge profiles at a current density of 0.1 A g^{-1}; (b) rate performance at a current density from 0.2 to 8.0 A g^{-1}; (c) cycling performance at a current density of 1 A g^{-1}; (d) schematic image of a full-cell at a voltage range from 0.5 to 4.5 V; (e) rate performances at a current density from 0.2 to 8 A g^{-1}; (f) Ragone plots of several full cell devices including the BNC//N-CM-6s device; (g) cycling performance at a current density of 1 A g^{-1}.

current density of 1 A g^{-1}. The BNC//N-CM-6s full cells retained approximately 66% of the initial capacity over 1,000 cycles, demonstrating their practicability.

4. Conclusion

N-CM-6s were fabricated from waste sawdust, a ubiquitous material. N-CM-6s had an amorphous carbon structure, high specific surface area of 3044 m^2 g^{-1}, nanoporous structure, and > 6 at.% heteroatoms. These properties enabled N-CM-6s to exhibit surface-driven charge storage behavior with a hybrid capacitive and pseudocapacitive reaction. In addition, a high capacity of 298 mAh g^{-1} and reversible cycles of more than 2,000 repetitive cycles can be achieved as a cathode for lithium-ion storage. In addition, in a full-cell test with the BNC anode, well-balanced energy, and power capabilities were achieved during 1,000 cycles. Therefore, this result reveals the successful upcycling of waste sawdust into nanostructured carbon materials that show high electrochemical performance.

Supporting information: Information is available regarding the experimental methods and results of H-CMs. The materials are available *via* the Internet at http://www.springer.com/13233.

References

(1) D. Larcher and J. M. Tarascon, *Nat. Chem.*, **7**, 19 (2015).
(2) N. Nitta, F. X. Wu, J. T. Lee, and G. Yushin, *Mater. Today*, **18**, 252 (2015).
(3) J. M. Tarascon and M. Armand, *Nature*, **414**, 359 (2001).
(4) P. Canepa, G. S. Gautam, D. C. Hannah, R. Malik, M. Liu, K. G. Gallagher, K. A. Persson, and G. Ceder, *Chem. Rev.*, **117**, 4287 (2017).
(5) D. Aurbach, B. D. McCloskey, L. F. Nazar, and P. G. Bruce, *Nat. Energy*, **1**, 16128 (2016).
(6) A. Manthiram, S. H. Chung, and C. X. Zu, *Adv. Mater.*, **27**, 1980 (2015).
(7) Z. J. Xie, X. Zhang, Z. Zhang, and Z. Zhou, *Adv. Mater.*, **29**, 1605891 (2017).
(8) W. Xu, J. L. Wang, F. Ding, X. L. Chen, E. Nasybutin, Y. Zhang, and J. G. Zhang, *Energy Environ. Sci.*, **7**, 513 (2014).
(9) J. B. Goodenough and Y. Kim, *Chem. Mater.*, **22**, 587 (2010).
(10) V. Etacheri, R. Marom, R. Elazari, G. Salitra, and D. Aurbach, *Energy Environ. Sci.*, **4**, 3243 (2011).
(11) M. S. Whittingham, *Chem. Rev.*, **104**, 4271 (2004).
(12) J. W. Fergus, *J. Power Sources*, **195**, 939 (2010).
(13) A. Manthiram, *J. Phys. Chem. Lett.*, **2**, 176 (2011).
(14) D. Chen, L. H. Tang, and J. H. Li, *Chem. Soc. Rev.*, **39**, 3157 (2010).
(15) L. M. Dai, D. W. Chang, J. B. Baek, and W. Lu, *Small*, **8**, 1130 (2012).
(16) K. Karuppasamy, J. Theerthagiri, D. Vikraman, C. J. Yim, S. Hussain, R. Sharma, T. Maiyalagan, J. Qin, and H. S. Kim, *Polymers*, **12**, 918 (2020).
(17) X. Wang, L. Liu, and Z. Niu, *Mater. Chem. Front.*, **3**, 1265 (2019).

(18) D. Vikraman, S. Hussain, K. Prasanna, K. Karuppasamy, J. Jung, and H. S. Kim, *J. Electroanal. Chem.*, **833**, 333 (2019).
(19) P. Kalyani and A. Anutha, *Int. J. Hydrog. Energy*, **38**, 4024 (2013).
(20) B. Hu, K. Wang, L. H. Wu, S. H. Yu, M. Antonietti, and M. M. Titirici, *Adv. Mater.*, **22**, 813 (2010).
(21) J. C. Wang and S. Kaskel, *J. Mater. Chem.*, **12**, 23710 (2012).
(22) N. R. Kim, H. J. An, Y. S. Yun, and H. J. Jin, *Carbon Lett.*, **12**, 110 (2017).
(23) R. R. Gaddam, D. F. Yang, R. Narayan, K. V. S. N. Raju, N. A. Kumar, and X. S. Zhao, *Nano Energy*, **26**, 346 (2016).
(24) B. Campbell, R. Ionescu, Z. Favors, C. S. Ozkan, and M. Ozkan, *Sci. Rep.*, **5**, 14575 (2015).
(25) P. Zheng, T. Liu, J. Z. Zhang, L. F. Zhang, Y. Liu, J. F. Huang, and S. W. Guo, *RSC Adv.*, **5**, 40737 (2015).
(26) Y. S. Yun, D. H. Kim, S. J. Hong, M. H. Park, Y. W. Park, B. H. Kim, H. J. Jin, and K. Kang, *Nanoscale*, **7**, 15051 (2015).
(27) A. G. Dumanli and A. H. Windle, *J. Mater. Sci.*, **47**, 4236 (2012).
(28) Y. S. Yun, H. Bak, and H. J. Jin, *Synth. Met.*, **160**, 561 (2010).
(29) N. R. Kim, S. M. Lee, M. W. Kim, H. J. Yoon, W. G. Hong, H. J. Kim, H. J. Choi, H. J. Jin, and Y. S. Yun, *Adv. Energy Mater.*, **7**, 1700629 (2017).
(30) E. Adelowo, A. R. Baboukani, C. Chen, and C. Wang, *C-J Carbon Res.*, **4**, 31 (2018).
(31) A. Lu, M. Chen, X. Wang, T. Xing, M. Liu, and X. Wang, *J. Power Sources*, **398**, 128 (2018).
(32) S. H. Lee, C. John, and P. S. Grant, *ACS Appl. Mater. Interfaces*, **11**, 37859 (2019).
(33) Y. Yang, Q. Lin, B. Ding, J. Wang, V. Malgras, J. Jiang, Z. Li, S. Chen, H. Dou, S. M. Alshehri, T. Ahamad, J. Na, X. Zhang, and Y. Yamauchi, *Carbon*, **167**, 627 (2020).
(34) S. J. Zhang, C. Li, X. Zhang, X. Z. Sun, K. Wang, and Y. W. Ma, *ACS Appl. Mater. Interfaces*, **9**, 17136 (2017).
(35) Q. Y. Xia, H. Yang, M. Wang, M. Yang, Q. B. Guo, L. M. Wan, H. Xia, and Y. Yu, *Adv. Energy Mater.*, **7**, 1701336 (2017).
(36) H. W. Wang, C. Guan, X. F. Wang, and H. J. Fan, *Small*, **11**, 1470 (2015).